Supporting Information

Gold Plasmon-Induced Photocatalytic Dehydrogenative Coupling of Methane to Ethane on Polar Oxide Surfaces

Lingshu Meng, Zhenye Chen, Zhiyun Ma, Sha He, Yidong Hou, Hao-Hong Li, Rusheng Yuan, Xi-He Huang, Xuxu Wang, Xinchen Wang, Jinlin Long*

State Key Lab of Photocatalysis on Energy and Environment, College of Chemistry, Fuzhou University, Fuzhou, 350116, P. R. China.

Email: jllong@fzu.edu.cn

Experimental Section.

1.1 Preparation of ZnO nanorods array and ZnO nanosheets array

0.06 g zinc acetate was added in 60 mL of ethanol solution, stirring for 30 minutes. After fully dissolved, the cleaned conductive glass (FTO) was faced downward, immersed in the solution for 10 seconds, then taken out, and dried with nitrogen. The impregnation-nitrogen dried step was repeated 5 times, and then the impregnated conductive glass was transferred to a muffle furnace, and the rate of temperature rise was controlled, and calcined at 623 K in an air atmosphere at a rate of 2 K/ min for 30 minutes to obtain zinc oxide seed crystal.

0.71 g zinc nitrate hexahydrate was added in 30 mL of deionized water to obtain solution A. 0.33 g hexamethylenetetramine was dissolved in 30 mL of deionized water to get the solution B. The A and B solutions were added slowly into a 100 mL Teflon autoclave and was stirred for 10 minutes. Then, the FTO with ZnO seed was placed in the above-mentioned mixed solution, and then transferred to a constant temperature oven. After heated at 368 K for 24 hours, the autoclave was taken out in air and cooled to room temperature. Finally, the ZnO nanorods array was rinsed repeatedly with ethanol and deionized water. The as-prepared sample was calcined at 673 K for 5 hours.

ZnO nanosheets arrays were synthesized by a modified hydrothermal procedure. Typically, an

indicated amount of $Zn(Ac)_2•2H_2O$ and $CO(NH_2)_2$ was dissolved firstly into deionized water, and then 0.083 g F-127 surfactant was added into the mixed 70 mL solution of 0.079 M $Zn(Ac)_2$ and 0.275 M $CO(NH_2)_2$, and finally 0.1 mol acetic acid was added to adjust pH = 4-5 and stirred continuously at the room temperature for 2 h. After the transparent solution was transferred into a dried Teflon-liner stainless steel autoclave with a volume of 100 mL, two pieces of FTO coated with ZnO seed were putted, in which the conducting side was downside. The autoclave was kept at 368 K for 24 h in an electric oven, and then cooled to room temperature. The as-prepared ZnO NS array samples (denoted as m-ZnO NSs) were washed with deionized water and ethanol for several times, dried at 353 K overnight, and finally calcined at 773 K for 10 h.

1.2 Preparation of Au/m-ZnO-x NSs

Au/m-ZnO NS arrays were prepared by a photodeposition method. The as-prepared ZnO NS arrays were immersed into 50 mL of $HAuCl_4•3H_2O$ aqueous solution and then irradiated with a Xe lamp to deposit Au NPs onto ZnO NSs for 30 min. The color of ZnO was gradually changed from white to light burgundy. The resultant sample was washed with deionized water and dried at 353K overnight. The content of Au was regulated by varying the dosage of $HAuCl_4•3H_2O$. The resultant sample was denoted as Au/m-ZnO-x, where x stands for the molar percentage of Au content (x = 1.2, 2.5, 4.8 and 7.3 mol%).

1.3 Characterization of Au/m-ZnO-x photocatalysts

XRD measurements were performed on a Bruker D8 Advance X-ray diffractometer equipped with a Cu Kα1 radiation (λ = 1.5406 Å). SEM images were taken with a Hitachi S-5800 system. TEM images were obtained by a JEOL model JEM 2010 EX instrument at the accelerating voltage of 200 KV. UV-Vis DRS spectra were measured on a Varian Cary 500 Scan UV-Vis-NIS spectrophotometer using $BaSO_4$ as a reference ranging from 200 to 800 nm. XPS data were carried out on an ESCALAB 250 XPS system with a monochromatized Al Kα X-ray source (15 KV, 200 W, 500 μm, pass energy = 20 eV). AFM images were recorded using an Agilent 5,500

AFM (Agilent Technologies, USA). Temperature programmed desorption (TPD) were performed on an Autochem 2910 automatic catalyst characterization system equipped with an Omnistar GSD 30103 mass spectrometer. The sample loading was 0.2000 g. The flow rate of the carrying gas (highly pure He (5N)) was 30 $cm^3 min^{-1}$ and the heating rate was 5 $Kmin^{-1}$. The electrochemical transient photocurrent response analysis was carried out on a ZENNIUM workstation, respectively. The analysis was performed in Na_2SO_4 (0.2 M), where an Ag/AgCl electrode was used as reference electrode and a Pt electrode was used as counter electrode. ESR signals of the radical spin-trapped by 5, 5-dimethyl-1-pyrroline-N-oxide (DMPO) were examined with a Bruker ESP 300E spectrometer. The freshly prepared DMPO solution (0.2 mol L^{-1}) and suspension of sample (5.0 mg) were mixed directly before their transfer into a cylindrical quartz tube (length 100 mm and diameter 2 mm). The EPR signals of the DMPO-$^{\bullet}OH$, DMPO-$O_2^{\bullet-}$, and DMPO-$^{\bullet}CH_2OH$ spin adducts were detected in water and methanol, respectively. A 300 W commercial Xe lamp was used as a photoexcitation light source, and the ESR spectra were recorded at room temperature. The settings for the EPR spectrometer were as follows: center field, 3510.00 G; microwave frequency, 9.79 GHz; power, 5.05 mW. ESR signals of the photocatalysts were also examined with a Bruker ESP 300E spectrometer. A 300 W commercial Xe lamp was used as a photoexcitation light source, and the ESR spectra were recorded at room temperature. The settings for the EPR spectrometer were as follows: center field, 3510.00 G; microwave frequency, 9.79 GHz; power, 5.05 mW.

2. Computational Methods

During the theoretical stimulation using density functional theory (DFT) calculations, the Vienna ab initio simulation package (VASP) code was employed,[1] and the exchange−correlation functions were treated by the Perdew−Burke−Ernzerhof (PBE) generalized gradient approximation (GGA).[2] The plane-wave basis set with a cutoff energy of 400 eV within the

projector augmented wave (PAW)[3,4] method was used. The inter-molecular interactions during the geometry optimizations were taken into account by using DFT-D2 method. An inverse model compared with Zn(001)/Au_n was used to investigated the effect of the golden cluster support on the ZnO toward CH_4 coupling reaction. According to experimental facts, the Au clusters are about 30 nm, so the Au(111) surface was modeled by a two-layer 4×4 unit cell. On Au(111) surface, a Zn_3O_3 cluster extracted from the first layer of Zn-terminated ZnO(001) was supported. And the Zn_3O_3 cluster was sealed by hydrogen atoms. The Brillouin-zone integration was performed on a grid of 1×1×1 Monkhorst−Pack special k-points. A vacuum layer of 20 Å thick was applied perpendicular to the slab to avoid artificial interactions between the slab and its periodic images. The accuracy in the energy convergence is set as 10^{-5} Ry. The adsorption energy (ΔE_{ads}) on the $Zn_3O_3H_3$/Au(111) clusters is defined as ΔE_{ads} = E[the intermediates]-(E[$Zn_3O_3H_3$/Au(111) clusters]+ E[methane or ethane]).

3. Mid-IR Femtosecond Transient Absorption

A Clark-MXR IR optical parametric amplifier was pumped with 1 mJ/pulse of the 800 nm fundamental beam to generate two tunable near-IR pulses from 1.1 to 2.5 μm (signal and idler, respectively). They were combined in a 1-mm-thick $AgGaS_2$ crystal to generate the mid-infrared probe pulses from 3 to 10 μm by difference frequency generation (DFG). The DFG signal was collimated with a 50 cm CaF_2 lens before it was focused into a 0.5 mm path length Harrick cell containing the sample, and near the focal point, it overlapped with the temporally delayed pump pulses with different wavelengths. The mid-IR probe was then dispersed in a monochromator and the intensity change of the IR light induced by photoexcitation was monitored as a function of time with a 32-element HgCdTe array detector. The pump beam was chopped by a Chopper at 500 Hz. The IRF of this spectrometer was determined to be ~260 fs by fitting signal formation time of quantum dots under band edge excitation.

4. Photocatalytic Activity Testing

The solar light activities for the photocatalytic C-C-coupling of methane was performed in a 40 mL Schlenk flask reactor with a silicone rubber septum under atmospheric pressure and ambient temperature. Loading of Au/m-ZnO NSs photocatalyst was ca. 1.0 mg. This system was first evacuated by a mechanical pump and then filled with Ar gas. The reactor was evacuated by a mechanical pump, purged and filled with Ar gas, evacuation-filling operation was repeated three

times. 1.0 bar of Ar was introduced with a syringe via the septum, and then 0.5 mL CH_4 gas was injected into the reactor. A 300 W commercial Xe lamp was used as an irradiation resource and vertically placed outside the reactor. Every 1 h, 0.5 mL of reactive gas were taken from the reactor with a syringe and analyzed by two GCs. An Agilent GC-7890A equipped with a flame ionized detector (FID) and a chromatographic column (GASPRO) was used for determination of C_2H_6, higher hydrocarbons, and alcohols. Another Agilent GC-7890B equipped with A TCD detector, a FID detector, a methane converter, and two chromatographic columns of MolSieve 5A and Porapak Q was used for determination of CO, CO_2 and H_2 gases.

The solar-to-chemical energy conversion (SCC) efficiency was calculated with Eq. 1

$$\text{SCC efficiency (\%)} = \frac{[\Delta G \text{ for } C_2H_6 \text{ production (J mol}^{-1})][C_2H_6 \text{ formed (mol}^{-1})]}{[\text{total input energy (W)}][\text{reaction time (s)}]} \times 100\%$$

The free energy for C_2H_6 generation is 68.6 kJ mol^{-1}. The overall irradiance of the Xe lamp (320～2500 nm) is 600 mW cm^{-2}, and the irradiation area is 5.0 cm^{-2}. The total input power over the irradiation area is therefore determined to be 3.0 W. The irradiance of the Xe lamp was measured by a light intensity meter (ILT950).

Table S1. Control experimental results of the methane coupling over the Au/m-ZnO-4.8 photocatalyst

Reactant	Catalyst	Sunlight	Products
—	√	√	none
CH_4	×	√	none
CH_4	√	×	none
CH_4	√	√	C_2H_6\H_2

Table S2. Calculated potential energies of formed intermediates for the methane coupling reaction on $Zn_3O_3H_3$(001)/Au(111), $Zn_3O_3H_3$(100)/Au(111) and $Zn_3O_3H_3$(001) models

Calculation Models	Calculated Energy (eV)	Total Energy (eV)	Normalized Energy (eV)	Adsorption Energy (eV)
$Zn_3O_3H_3$(001)/Au(111)	-155.6871	-203.7359	0	0
Au-ZnO-CH_3-H (IM1)	-179.3521	-203.3765	+0.3594	+0.3594
Au-ZnO-C_2H_6 (IM2)	-196.5602	-203.3508	+0.3858	-0.4291
$Zn_3O_3H_3$(001)/Au(111)+C_2H_6+H_2	-202.9217	-202.9217	+0.8149	–
$Zn_3O_3H_3$(100)/Au(111)	-149.0220	-197.0708	0	0
$Zn_3O_3H_3$(100)/Au(111)-CH_3-H (IM1)	-172.9257	-196.9501	+0.1198	+0.1207
$Zn_3O_3H_3$(100)/Au(111)-C_2H_6 (IM2)	-189.7564	-196.547	+0.5238	-0.2911
$Zn_3O_3H_3$(100)/Au(111)+C_2H_6+H_2	-196.2559	-196.2559	+0.8149	–
$Zn_3O_3H_3$(001)	-173.3804	-221.4292	0	0
ZnO-CH_3-H (IM1)	-198.5831	-222.6075	-1.1783	+1.1783
ZnO-C_2H_6 (IM2)	-217.8843	-218.9945	+2.4347	-2.9504
$Zn_3O_3H_3$(001) +C_2H_6+H_2	-220.6143	-220.6143	+0.8149	–

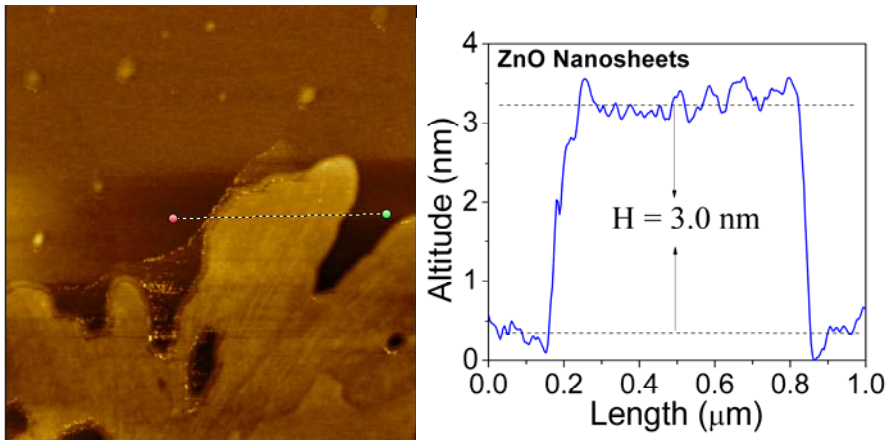

Figure S1. AFM image of bare m-ZnO NSs.

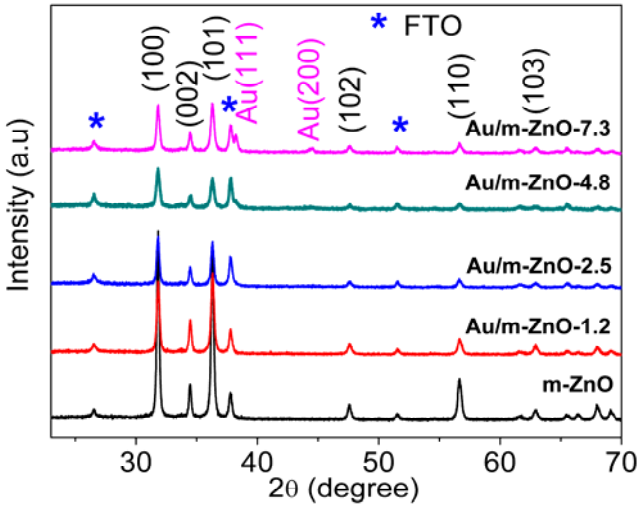

Figure S2. XRD patterns of the bare m-ZnO and Au/m-ZnO-x samples.

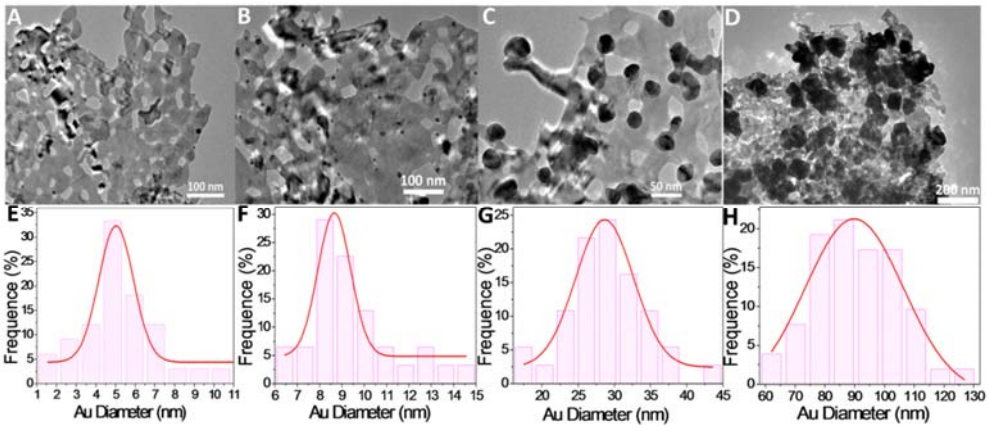

Figure S3. TEM images and Au size distributions of Au/m-ZnO-1.2 (A, E), Au/m-ZnO-2.5 (B, F), Au/m-ZnO-4.8 (C, G), and Au/m-ZnO-7.3 (D, H) samples

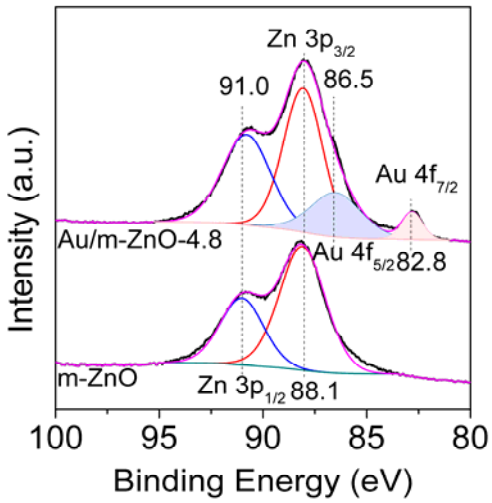

Figure S4. XPS analysis of the bare m-ZnO and Au/m-ZnO-4.8 samples

We applied X-ray photoelectron spectroscopy (XPS) to characterize the surface electronic structure of the Au/m-ZnO-4.8 photocatalyst, as shown in Figure S4. The two 4f binding energies of the metallic Au NPs, corresponding to $4f_{5/2}$ and $4f_{7/2}$ at 86.5 and 82.8 eV, far lower than those of bare Au NPs[5]. The significant shift towards lower energy indicates the enhanced electron density of Au NPs, which is attributed to the electron transfer from the ZnO NSs to the Au NPs.

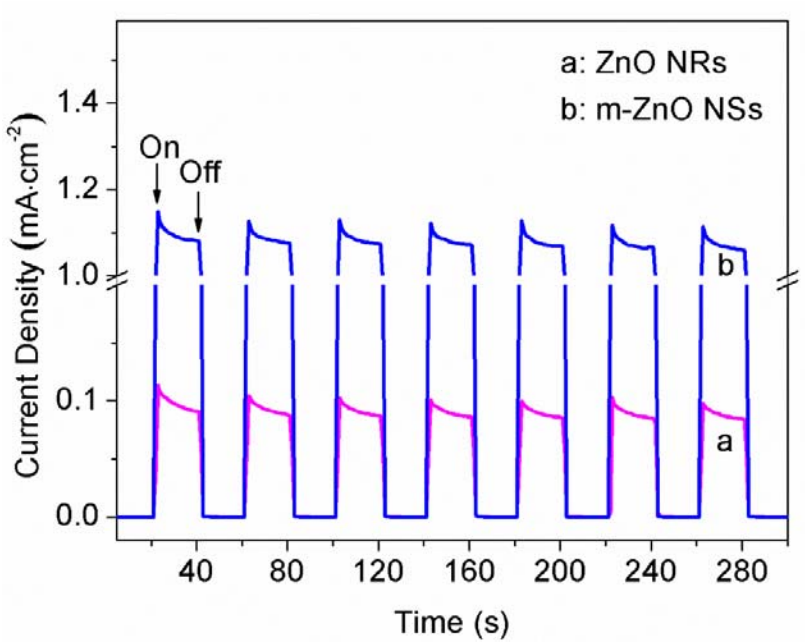

Figure S5. Comparison of photocurrent responses of m-ZnO NSs (b) and nanorods (a) arrays in 0.2 M Na_2SO_4 solution under sunlight light.

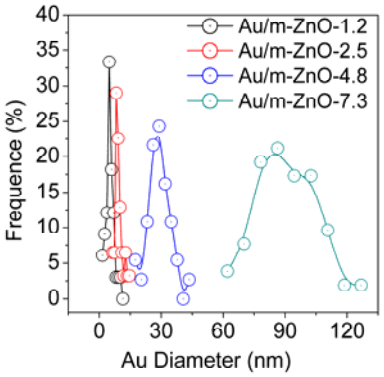

Figure S6. Size distribution of Au nanoparticles in Au/m-ZnO-x samples.

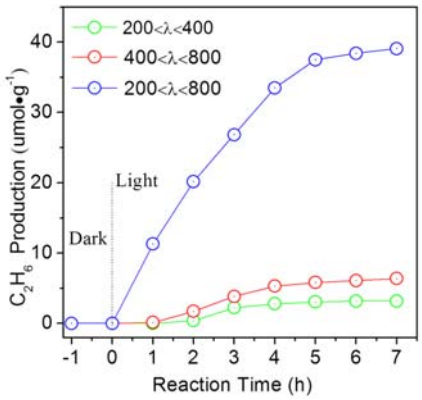

Figure S7. Ethane production functions as irradiation time using the Au/m-ZnO-4.8 photocatalyst under different light wavelengths (CH_4: 22.3 umol).

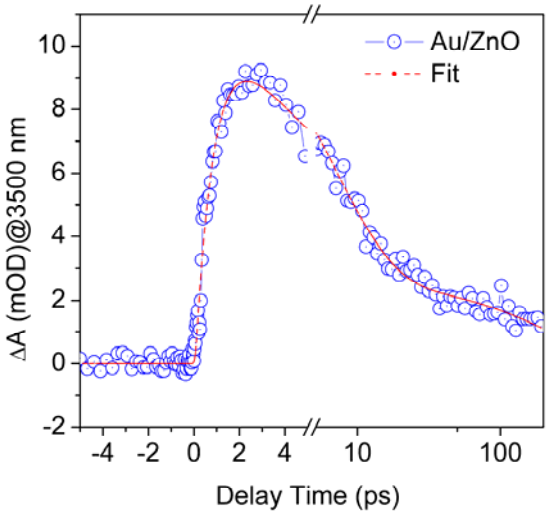

Figure S8. Electron decay kinetics at 3500 nm over Au/ZnO film. Fit curves are shown by dotted line.

The electron injection trace is fitted by an equation of $y = a(1+e^{t/\tau 0})$, where τ0 represents the half time of electron injection to conduction band of ZnO NSs. The decay trace is fitted by the bi-exponential function: $y = a_1e^{t/\tau 1}+a_2 e^{t/\tau 2}$, where τ1 and τ2 represent the lifetime of fast decay component and slow decay component, respectively. It can be calculated that τ_0, τ_1, and τ_2 are equal to 0.9, 6.7, and 231.5 ps, respectively.

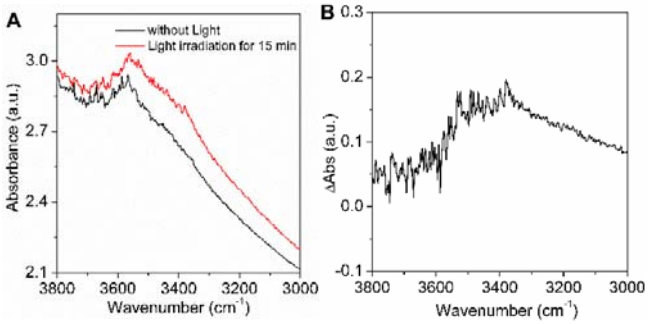

Figure S9. (A) In situ FTIR spectra under methane atmosphere of Au/ZnO-4.8 sample dehydrated under vacuum at 673 K. (B) the difference spectra before and after light irradiation. It can appear from Figure S9A that a broad band centered at ca. 3550 cm^{-1} is due to surface isolated hydroxyls. After 15 min of light irradiation. The intensity of these bands is enhanced significantly. We plotted the difference (ΔA) spectrum of Au/ZnO-4.8 photocatalyst before and after light irradiation, as displayed in Figure S9B. The amount of surface isolated hydroxyls is increased greatly by solar light irradiation, which is a direct evidence for the formation of OH species, along with the dissociation of methane.

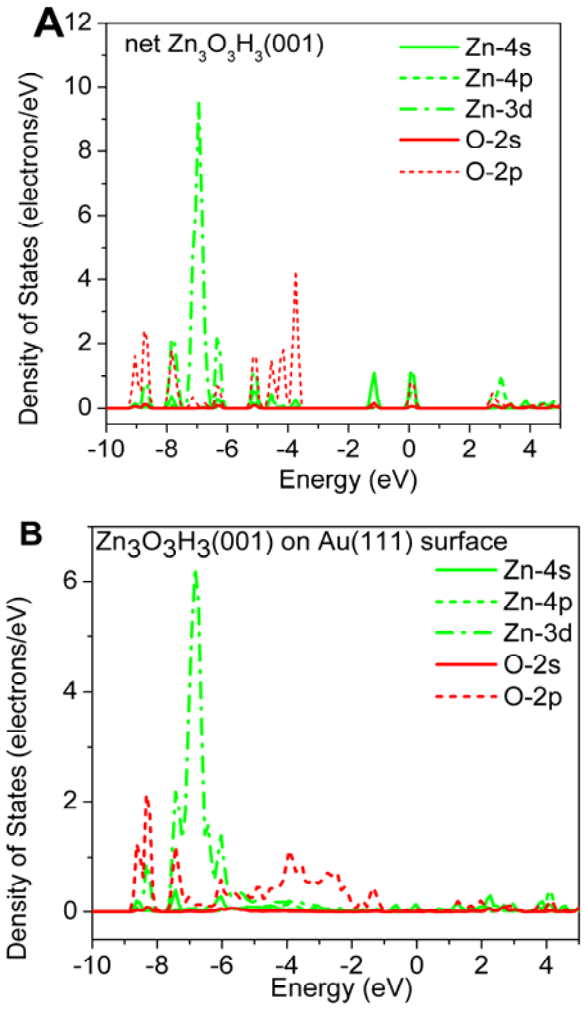

Figure S10. PDOS of the $Zn_3O_3H_3$(001) cluster before (A) and after (B) deposition on Au(111) surface.

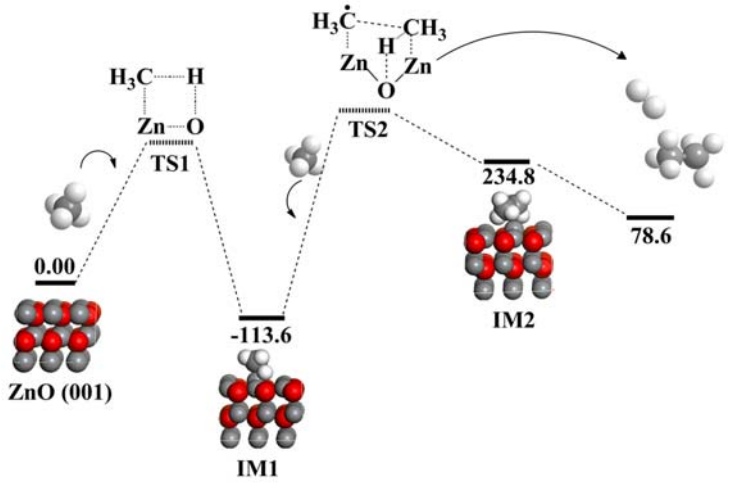

Figure S11. Potential energy diagram for the methane coupling reaction on $Zn_3O_3H_3(001)$ (energy in kJ mol^{-1}).

The density functional theory (DFT) was used to calculate the potential energy diagram of the methane coupling reaction on $Zn_3O_3H_3(001)$ clusters (extracted from polar Zn(001) surface), especially the two intermediates (IM1, IM2). It can appear that the exposed Zn^{2+} sites at the metal/metal oxide interface can directly react with methane molecules to form the stable Zn-CH_3 species (IM1). The process is thermodynamically favorable. However, the IM2 formation is thermodynamically unfavorable. It needs a large Gibbs free energy as high as +350 kJ mol^{-1}, thus one can conclude that ethane can not be produced on the alone ZnO plane at this stage owing to the large energy barrier. Interestingly, compared with $Au/Zn_3O_3H_3(001)$ cluster, the introduction of plasmonic Au NPs thermodynamically unfavorable to the formation of the IM1 intermediate, but facilitates to generate the IM2. That is, Au plasmon can reduce significantly the thermodynamic energy barrier of C-C coupling step, improving the final production of ethane.

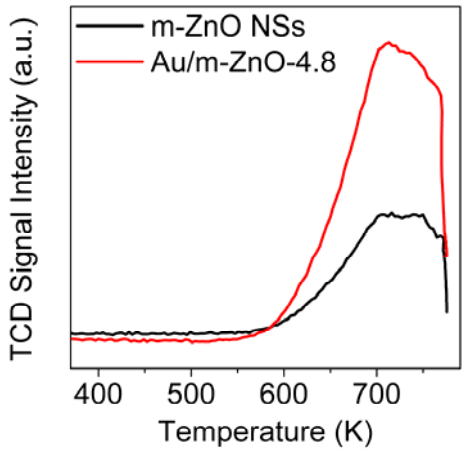

Figure S12. CH_4-TPD patterns of bare m-ZnO and Au/m-ZnO-4.8 photocatalysts.

Figure S12 shows the TPD results of methane adsorbed on bare m-ZnO and Au/m-ZnO-4.8 photocatalysts. It can be seen that there is only one desorption peak at the temperature range of 550-773 K. The peak centered at ca. 700 K is attributed to the desorption of chemically adsorbed methane molecules. Comparison of the peak intensity finds that plasmonic Au NPs significantly enhanced the chemical adsorption of methane on ZnO NSs. This result, together with the DFT calculation on charge transfer between ZnO and Au NPs, indicates conclusively that the electric field coupling improved the dissociation of C-H bonds in methane on THE {001} plane of ZnO NSs.

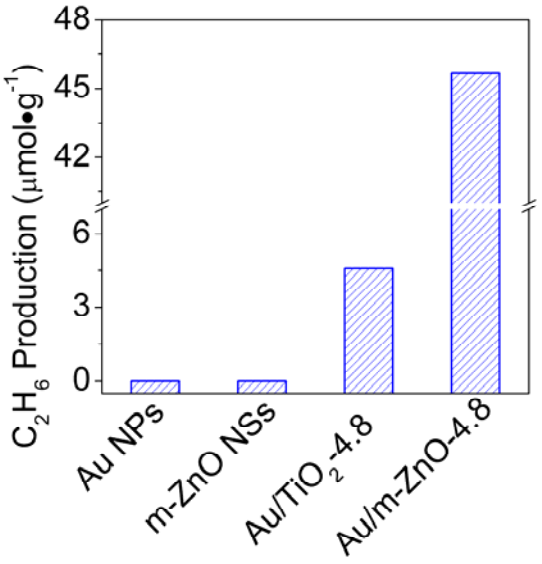

Figure S13. Comparison of Au/TiO_2-4.8 and Au/m-ZnO-4.8 photocatalysts for the methane coupling under solar light irradiation.

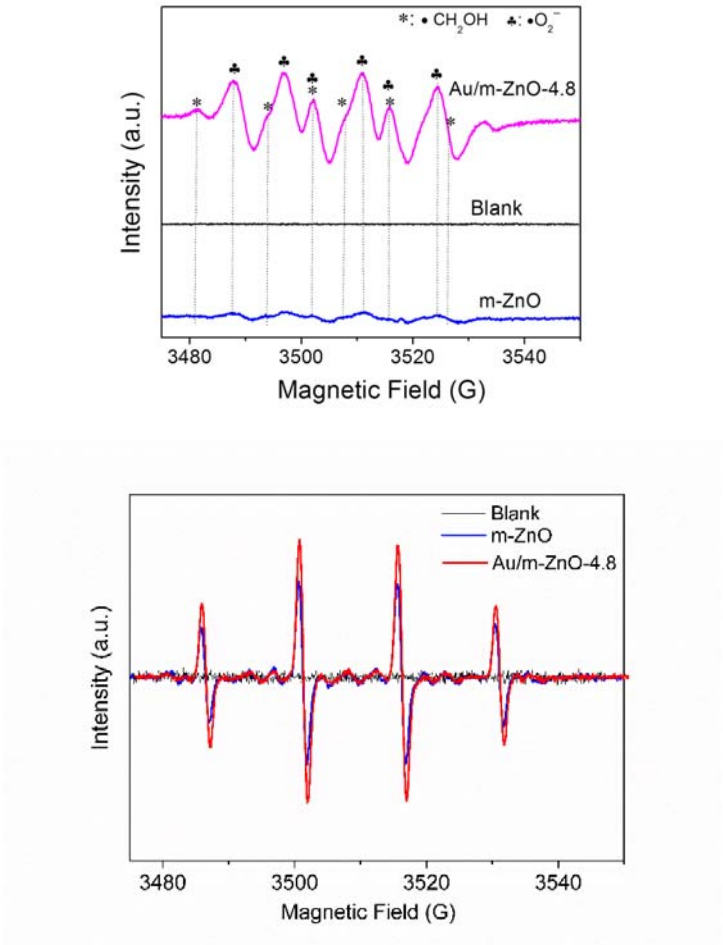

Figure S14. Spin trapping ESR spectra at 298K of DMPO-•OH adduct generated on the m-ZnO and Au/m-ZnO-4.8 photocatalysts with solar light excitation.

The several characteristic EPR signals assigned to the DMPO-•O_2- and DMPO-•CH_2OH adducts indicate the formation of •O_2- radical and •CH_2OH radicals by the electron reduction of O_2 molecules and by the hole oxidation of water.[6] Au/m-ZnO-4.8 gives a stronger ESR line intensity compared to m-ZnO, indicating that the more amounts of photogenerated electrons and holes are separated and transported to the surface of ZnO NSs under the Au SPR field.

1. G. Kresse, Furthmüller, *J. Phys. Rev. B.* 1996, **54**, 11169.

2. J. P. Perdew, K. Burke, M. Ernzerhof. *Phys. Rev. Lett.* **1996**, **77**, 3865.

3. G. Kresse, D.Joubert. *Phys. Rev. B.* 1999, **59**,1758.

4. P. E. Blochl. *Phys. Rev. B.* 1994, **50**, 17953.

5. M. Behl, P. K. Jain. *Angew. Chem. In. Ed.* 2015, **54**, 992; *Angew Chem*, 2015, **127**, 1006.

6. Q. Gu, J. L. Long, L. Z. Fan, L. M. Chen, L. L. Zhao, H. X. Lin, X. X.Wang. *J. Catal.* 2013, **303**, 141.